Journal of Alloys and Compounds 880 (2021) 160553

Contents lists available at ScienceDirect

Journal of Alloys and Compounds

journal homepage: www.elsevier.com/locate/jalcom

Orientation dependence of elastocaloric effect in $Ni_{50}Mn_{30}Ga_{20}$ single crystals

N.Yu. Surikov*, E.Yu. Panchenko, E.E Timofeeva, A.I. Tagiltsev, Yu.I. Chumlyakov

National Research Tomsk State University, Tomsk 634050, Russian Federation

ARTICLE INFO

Article history:
Received 25 March 2021
Received in revised form 20 May 2021
Accepted 22 May 2021
Available online 26 May 2021

Keywords:
NiMnGa single crystals
Martensitic transformation
Superelasticity
Elastocaloric effect
Stress hysteresis

ABSTRACT

In this study, the orientation dependence of the elastocaloric effect and superelasticity in $Ni_{50}Mn_{30}Ga_{20}$ single crystals undergoing $L2_1$–10M/14M–$L1_0$ martensitic transformations was investigated. The maximum value of the adiabatic temperature change ΔT_{ad} at reverse stress-induced martensitic transformations was shown to weakly depends on the orientation and equals 10.8 and 12.3 K in compression along the [001] and [011] directions, respectively. The superelasticity and elastocaloric effect temperature intervals were determined from the crystal orientation and were 80 K from 373 to 453 K for [001]-oriented crystals and 30 K from 373 to 403 K for [011]-oriented crystals. The strong orientation dependence of stress hysteresis $\Delta\sigma$ ($\Delta\sigma$ = 50–60 MPa for [001]-oriented crystals and $\Delta\sigma$ = 110–142 MPa for [011]-oriented crystals) did not significantly affect the ΔT_{ad}, but determined the efficiency of the material for practical use as a solid state cooling device. The factors influencing the $\Delta T_{ad}(T)$ dependence were analyzed.

© 2021 Elsevier B.V. All rights reserved.

1. Introduction

In recent years, ferromagnetic shape memory alloys have attracted great interest as promising materials for solid-state cooling methods based on the elastocaloric effect (ECE). In shape memory alloys, elastocaloric cooling consists of the adiabatic temperature change ΔT_{ad} during the reverse endothermic stress-induced martensitic transformation (MT) at superelasticity (SE) conditions [1–3].

Heusler NiMnGa- and NiFeGa-based alloys undergoing intermartensitic $L2_1$–10M/14M–$L1_0$ MT are one of the promising materials with potential in research and application of elastocaloric properties due to the large ΔT_{ad} values (up to 9.0–13.5 K), low deforming stresses (150–350 MPa), narrow stress hysteresis, high coefficient of performance (COP) up to 20 and high cyclic stability of the ECE (stable elastocaloric behavior with a little degradation for > 250 loading/unloading cycles) [4–10]. Both narrow stress hysteresis, responsible for energy dissipation, and low deformation stresses (150–350 MPa), required to complete stress-induced MT, increase the efficiency and facilitate the design of solid-state refrigerators. In addition, the possibility of combining elastocaloric and magnetocaloric effects may significantly expand the application of the cooling ability of ferromagnetic shape memory alloys [11].

Research to date has shown that a directionally solidified $Ni_{55}Mn_{18}Ga_{27}$ alloy with a strong $<100>_A$ preferred orientation displays large adiabatic temperature change values up to ΔT_{ad} ~ 10.7 K [8]. However, studies investigating the ECE in NiMnGa single crystals have not yet been carried out. The following fundamental problems, therefore, remain to be solved: determining the maximum resource of ΔT_{ad} of the alloy, identifying the orientation dependence of the ECE and establishing the relationship between the ECE and the thermomechanical properties of the alloy. It is known that a whole set of characteristics depends on the crystallographic orientation and can affect the ECE parameters. In Heusler NiMnGa- and NiFeGa-based alloys with intermartensitic $L2_1$–10M/14M –$L1_0$ MT, the yield stress of martensite and austenite, the stress hysteresis, and the contribution of martensite detwinning to reversible strain during stress-induced MT strongly depend on the crystal orientation [9,10]. These parameters determine the value of energy dissipation and thus both the ΔT_{ad} value and the cyclic stability of the ECE. Studying the dependence of the ECE on orientation in single crystals allows for excluding the influence of grain boundaries and determining the efficiency of the material for using the ECE, as well as developing a strategy for optimizing the elastocaloric properties. In the light of the foregoing, the purpose of this work is to study the influence of test temperature and crystallographic orientation on the ECE during stress-induced $L2_1$–10M/14M–$L1_0$ MT in $Ni_{50}Mn_{30}Ga_{20}$ (at%) single crystals in compression.

* Corresponding author.
E-mail address: Jet_n@mail.ru (N.Y. Surikov).

https://doi.org/10.1016/j.jallcom.2021.160553
0925-8388/© 2021 Elsevier B.V. All rights reserved.

2. Materials and methods

$Ni_{50}Mn_{30}Ga_{20}$ (at%) single crystals were grown using the Bridgman method in an inert gas atmosphere. MT temperatures were determined from the temperature dependence of the electrical resistance and by differential scanning calorimetry (DSC) using a NETZSCH DSC 404 F1 calorimeter. The specific heat ΔH, entropy ΔS for the MT and heat capacity at constant pressure C_p were determined according to standard methods based on the results of a DSC study, as, for example, in [12]. Transmission electron microscopic (TEM) studies were performed on a transmission electron microscope Hitachi HT-7700. The compression samples with dimensions of 3 mm × 3 mm × 6 mm were cut using electro-discharge machining. Mechanical tests were carried out on an Instron 5969 electromechanical testing machine. Sample strain was measured using common Instron 5969 sensor and controlled by the ASTM E83 clip-on extensometer. Errors in strain and stress measurements during mechanical tests were 0.2% and 2 MPa, respectively.

The ΔT_{ad} value was determined by directly measuring the temperature of the sample with a highly sensitive T-type thermocouple during mechanical testing at several temperatures. Thermocouple was attached to the samples during mechanical testing through thermoconductive paste. The scheme of mechanical tests with ECE (ΔT_{ad}) registration consisted of the following stages: loading the sample with a low strain rate under conditions close to isothermal until the specified stress was reached, which is necessary to complete the forward stress-induced MT. The stress level was then held for 10 s while the temperature of the sample was restored to the test temperature. After holding, the sample was unloaded with a high strain rate to ensure conditions closed to adiabatic. The results of the ECE study in as-grown $Ni_{50}Mn_{30}Ga_{20}$ single crystals are presented for loading/unloading cycles, which were carried out at the loading rate $\dot{\varepsilon} = 2.0 \cdot 10^{-3}$ s^{-1} and unloading rates $\dot{\varepsilon}_1 = 3.3 \cdot 10^{-2}$ s^{-1} and $\dot{\varepsilon}_2 = 6.7 \cdot 10^{-1}$ s^{-1}. The ECE measuring error was 0.5 K. The temperature-time data were recorded simultaneously with stress and strain data using a data acquisition module.

For the study, we selected as-grown $Ni_{50}Mn_{30}Ga_{20}$ single crystals, oriented along the $[001]_{L21}$- and $[011]_{L21}$-directions. The orientation of the single crystals was determined using a DRON-3 diffractometer with $Fe_{K\alpha}$ radiation. Along both $[001]_{L21}$- and $[011]_{L21}$-directions, the full theoretical transformation strain at $L2_1$–(10M/14M)–$L1_0$ MT in compression is $\varepsilon_{tr} = 5.8\%$, which is generally caused by the appearance of a twinned martensite ε_{CVP} and its subsequent detwinning ε_{detw} under stress ($\varepsilon_{tr} = \varepsilon_{CVP} + \varepsilon_{detw}$). The theoretical transformation strain was calculated using the phenomenological theory of the crystallography martensitic transformation [13,14]. For calculations the following $Ni_{50}Mn_{30}Ga_{20}$ lattice parameters were used: $a_0 = 0.5815$ nm for $L2_1$ austenite, and a = 0.7753 nm, c = 0.6598 nm for $L1_0$ martensite [15]. As has been shown on $[001]_{L21}$-oriented single crystals of Heusler alloys with $L2_1$–(10M/14M)–$L1_0$ MT, $L1_0$ martensite detwinning does not contribute to stress-induced MT ($\varepsilon_{detw} = 0$, $\varepsilon_{CVP} = \varepsilon_{tr}$). In these crystals, SE is characterized by narrow stress hysteresis (20–40 MPa) and high yield stress of austenite and martensite [8,10]. On the other hand, along the $[011]_{L21}$ direction, the contribution of $L1_0$ martensite detwinning to the total transformation strain is 50% ($\varepsilon_{detw} = 2.9\%$, $\varepsilon_{CVP} = 2.9\%$). Therefore, SE is accompanied by high values of energy dissipation and, accordingly, wide stress hysteresis up to 150–300 MPa [8,10]. This orientation makes it possible to elucidate the effect of $L1_0$-martensite detwinning and stress hysteresis on ECE characteristics.

3. Results and discussion

DSC curves and the temperature dependence of electrical resistance (ρ(T)) are shown in Fig. 1. Using these two methods for determining MT temperatures, studies were carried out showing the presence of two stages of forward and reverse MT and demonstrated a good coincidence of the characteristic MT temperatures (M_S, M_F, A_S, A_F). MT temperatures, specific heat capacity (C_p), values of specific heat ΔH and entropy ΔS for the full two-step $L2_1$–(10M/14M)–$L1_0$ forward (ΔH^{A-M}, ΔS^{A-M}) MT and reverse (ΔH^{M-A}, ΔS^{M-A}) MT are shown in Table 1. The staging observed on the DSC and ρ(T) curves in the temperature range 323–373 K in $Ni_{50}Mn_{30}Ga_{20}$ single crystals is associated with the $L2_1$–$L1_0$ MT through 10M/14M modulated structures in stress-free cooling/heating cycles (Fig. 1). This proposition is based on [16–18], where the existence of several DSC and internal friction peaks during the heating/cooling cycles is observed due to the multistep transformation from $L2_1$–phase to $L1_0$–phase through intermartensitic modulated structures. Moreover, a previous study on NiMnGa concluded that $L2_1$–10M/14M MT occurred with a smaller value of the specific heat ΔH (about 4.0 J/g) compared to during the formation of non-modulated $L1_0$-martensite, for which ΔH = 7.0 J/g [19]. As indicated in Table 1, the ΔH and ΔS values of the $Ni_{50}Mn_{30}Ga_{20}$ crystals were close to those obtained earlier for various NiMnGa alloys of similar compositions with $L2_1$–(10M/14M)–$L1_0$ MT: 6.3–7.4 J/g and 15.2–16.4 J/(kg·K), respectively [19–21]. The calculated value $C_p = 485$ J/(kg·K) coincided with values previously obtained within 5% error [21,22].

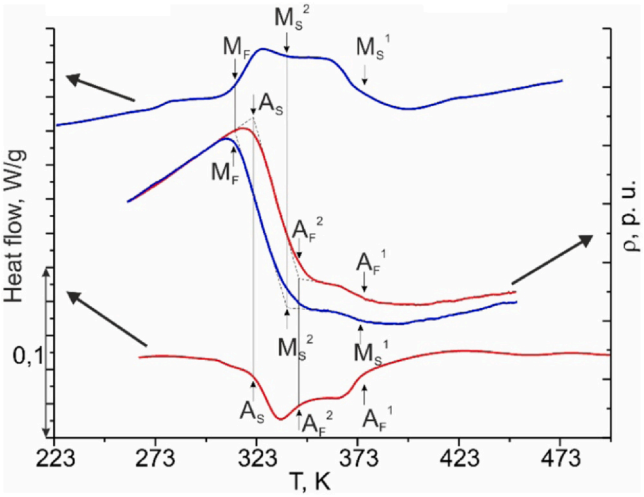

Fig. 1. Temperature dependence of electrical resistance and DSC curves for $Ni_{50}Mn_{30}Ga_{20}$ single crystals.

TEM observations confirmed that at room temperature (below the M_F) the material was in the $L1_0$-martensitic phase (Fig. 2). $L1_0$-martensite exhibits twinning along $\{111\}_{L10}$ planes in select electron diffraction patterns. The dark-field image in the $(11\bar{1})_{tw}$ reflection confirmed the presence of twins with a thickness of 10–50 nm.

Figs. 3 and 4 show the stress-strain curves during mechanical tests and the corresponding time-temperature curves ΔT(t) (changes in the sample temperature in the loading/unloading cycles) in [001]- and [011]-oriented $Ni_{50}Mn_{30}Ga_{20}$ single crystals. The temperature dependences of the ΔT_{ad} values corresponding to the maximum transformation strains are shown in Fig. 5. At low temperatures $A_S < T_t < A_F^1$, partial reversible strain during the MT in the loading/unloading cycle was observed. In [011]-oriented single crystals at $T_t < A_F^1$, the curves were characterized by distinct stages, which indicate the successive processes of stress-induced intermartensitic $L2_1$–10M/14M–$L1_0$ MT (Fig. 4). On the first stage in temperature range $T_t < A_F^1$, the reorientation and formation of 10M/14M layered modulated structures occurred under low critical stress, and given strain remains partially irreversible after unloading and recovers only after heating to $T_t > A_F^1$. At the temperature range $A_F^2 \le T_t < A_F^1$, the stress-induced $L1_0$-martensite formed during the second stage

Table 1
Characteristic parameters of MT and heat characteristics of as-grown $Ni_{50}Mn_{30}Ga_{20}$ single crystals.

M_S^1, K	M_S^2, K	M_F, K	A_S, K	A_F^1, K	A_F^2, K	ΔH^{A-M}, J/g	ΔH^{M-A}, J/g	ΔS^{A-M}, J/(kg·K)	ΔS^{M-A}, J/(kg·K)	C_p, J/(kg·K)
374	337	312	321	378	344	-9.3	7.1	-22.3	15.6	485

was thermodynamically unstable, and reversible strain was observed during unloading (Fig. 4, second curve).

In [001]-oriented crystals in the temperature range $A_S < T_t < A_F^1$, the stress hysteresis $\Delta\sigma \approx 50$ MPa exceeded the low critical stresses of martensite formation $\sigma_{cr} \approx 35$ MPa; therefore, in loading/unloading cycles at $A_F^2 \le T_t$, $L1_0$-martensite undergoes reverse transformation only after unloading and significant additional heating up to $T > A_F^1$ (Fig. 3). In the temperature range $A_S < T_t < A_F^1$, regardless of the crystal orientation, an increase in the ECE value upon unloading the sample (adiabatic change in the sample temperature ΔT_{ad}) was observed accompanied by an increase in the test temperature and reversible strain. The growth of the ΔT_{ad} occurs due to an increase in the volume fraction of the material undergoing reverse MT during unloading (Figs. 3–5).

The temperature range of SE with completely reversible strain and, accordingly, the operating temperature range of the ECE were observed at $T_t > A_F^1$ and depended on the crystal orientation. Single crystals oriented along the [001]-direction were characterized by a wider operating temperature range of the ECE – 80 K, from 373 to 453 K – compared with [011]-oriented single crystals, which had an ECE temperature range of 30 K: from 373 to 403 K. Such SE temperature interval dependence was observed in all single crystals of Heusler alloys with $L2_1$–(B2)–$L1_0$ MT [8–10]. The wide temperature range of SE in [001]-oriented crystals has been demonstrated to result from low critical stresses of martensite formation, narrow stress hysteresis, and high strength properties of austenite and martensite, compared with [011]-oriented crystals [8–10].

The maximum ΔT_{ad} value was observed at the beginning of the SE temperature range (373–393 K) and equaled 8.9 K and 10.8 K for the [001]-oriented and 11.3 K and 12.3 K for the [011]-oriented $Ni_{50}Mn_{30}Ga_{20}$ single crystals at unloading rates $\dot{\varepsilon}_1$ and $\dot{\varepsilon}_2$, respectively (Table 2). The ΔT_{ad} gradually decreased with a further increase in the test temperature $T_t > 393$ K.

The maximum value of adiabatic temperature change during ECE for a material with a thermoelastic MT can be estimated from the following relationship [2,6]:

$$\Delta T_{ad} \approx \frac{\Delta H}{C_p} = \frac{T\Delta S}{C_p}. \quad (1)$$

The values of specific heat and entropy, calculated from the DSC curves during the cooling/heating cycle in a stress-free state, do not depend on the orientation of the single crystals. Hence, the maximum theoretical ΔT_{ad} value in the first approximation should not depend on the orientation of the compression axis. Since the adiabatic cooling of the material occurs during the reverse MT, therefore, we used the specific heat and entropy values for the reverse transformation ΔH^{M-A} to estimate the ECE resource (Table 1). The maximum theoretical value of ΔT_{ad} for $Ni_{50}Mn_{30}Ga_{20}$ single crystals was $\Delta T_{ad}(max) = 14.5$ K. The maximum experimental values $\Delta T_{ad} = 12.3$ K were 2.2 K lower than the theoretical estimation of the adiabatic cooling value ΔT_{ad} (max) in the studied crystals (Table 2). This can be explained by technical factors (heat removal by capture) and deviation from adiabatic conditions during the reverse MT.

It was experimentally established that the ΔT_{ad} mainly depends on the SE transformation strain ε_{SE} and correspondingly on the volume fraction of stress-induced martensite. In the [001]-oriented $Ni_{50}Mn_{30}Ga_{20}$ single crystal, where the detwinning of $L1_0$-martensite under stress is absent, the martensite volume fraction is unequivocally characterized by SE strain – the larger the volume fraction of martensite, the larger the adiabatic temperature change. Fig. 3 ($\sigma(\varepsilon)$ curve at $T_t = 373$ K) shows that the growth of ΔT_{ad} value with strain was observed in [001]-oriented crystals not only at the II stage (where the deformation strengthening coefficient $\theta_{II} = |d\sigma|/|d\varepsilon|$ is low: 1.3–2.4 GPa) but also at the III stage (where the such coefficient is high $\theta_{III} = 14.1 - 13.2$ GPa). This indicates that the III stage is affected by both the elastic strain of formed martensite and the increase of martensite volume fraction at stress-induced MT. To finish the stress-induced MT in [001]-oriented $Ni_{50}Mn_{30}Ga_{20}$ single crystals, additional energy is required which leads to a higher coefficient of deformation strengthening θ as well as significant growth of stresses.

In [001]-oriented single crystals, the reversible SE strain ε_{SE} decreases with increasing temperature while the coefficient θ increases (Figs. 3 and 6). This SE strain to temperature response has been observed in many [001]-oriented single crystals of Heusler alloys in compression [9,10]. This is caused by several factors. First, the transformation strain decreases with the increase in temperature due to the difference between austenite E_A and martensite E_M elastic moduli. If $E_A < E_M$, which has been observed in these crystals, the SE strain decreases with the increase in temperature and deforming stresses [9,10,23]. The maximum SE strain ε_{SE} 3.5% for [001]-oriented single crystals and 4.1% for [011]-oriented crystals is less than the

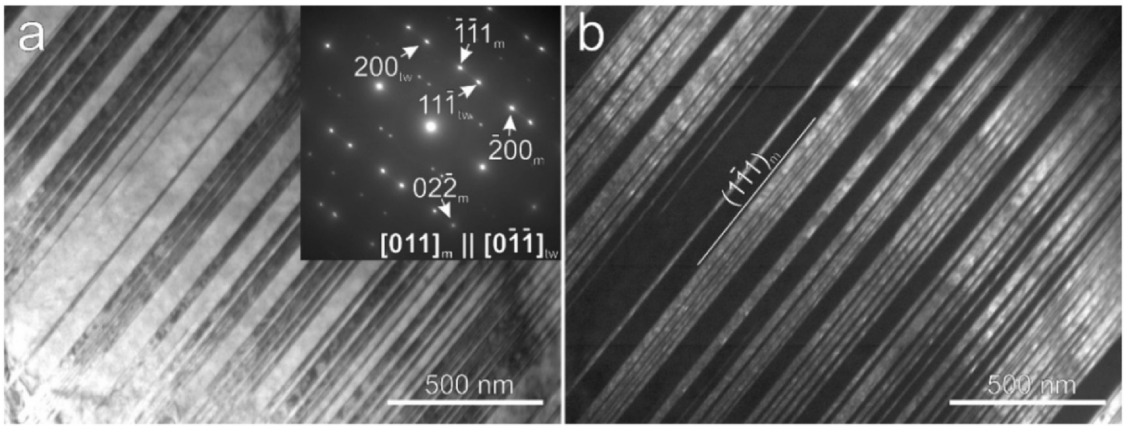

Fig. 2. Bright-field image, the corresponding select electron diffraction pattern (a) and dark-field image in the $[1\bar{1}1]_{tw}$ reflection (b) of twinned $L1_0$-martensite (zone axis $[011]_m||[0\bar{1}\bar{1}]_{tw}$) in $Ni_{50}Mn_{30}Ga_{20}$ single crystals.

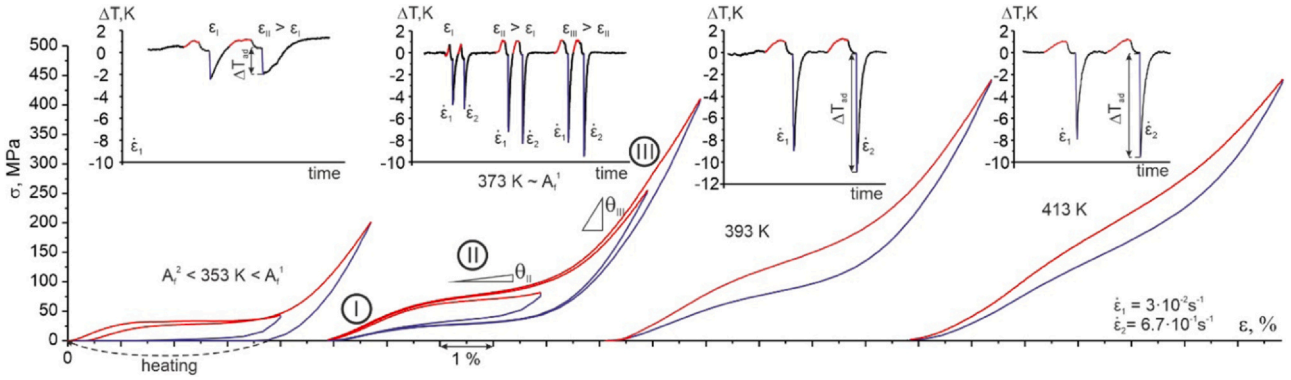

Fig. 3. σ(ε) curves and corresponding sample temperature change as a function of time ΔT(t) in the loading/unloading cycles for [001]-oriented $Ni_{50}Mn_{30}Ga_{20}$ single crystals in compression.

theoretical strain ε_{tr} = 5.8%. This is typical not only for NiMnGa crystals [6,17], but also for other single crystals of Heusler alloys [9,10]. Second, the MT in loading/unloading cycles at T_t higher than 413 K occurred in one stage with the high coefficient θ = 9.1 GPa, which increased with temperature. A high deformation strengthening coefficient θ results in a high value of applied stresses for complete stress-induced MT. Because the finish point of the stress-induced MT is not reached on the stress-strain response, than the martensite volume fraction may not achieve 100%, resulting in the reduction of strain ε_{SE} and the change of adiabatic temperature ΔT_{ad}. This effect gets stronger with the increase in temperature (Figs. 3, 5a and 6a).

The temperature interval of SE in [011]-oriented single crystals is 2.67 times lower than the interval in [001]-oriented crystals; thus, the deformation strengthening coefficient θ does not increase with temperature. In such a narrow temperature interval (30 K), the SE strain ε_{SE} and ΔT_{ad} weakly depend on the test temperature (Figs. 5b and 6b).

It should be noted that the increase in unloading rate from $\dot{\varepsilon}_1 = 3.3\cdot10^{-2}$ s^{-1} to $\dot{\varepsilon}_2 = 6.7\cdot10^{-1}$ s^{-1} resulted in significant growth of ΔT_{ad} by 18% in [001]-oriented $Ni_{50}Mn_{30}Ga_{20}$ single crystals, in

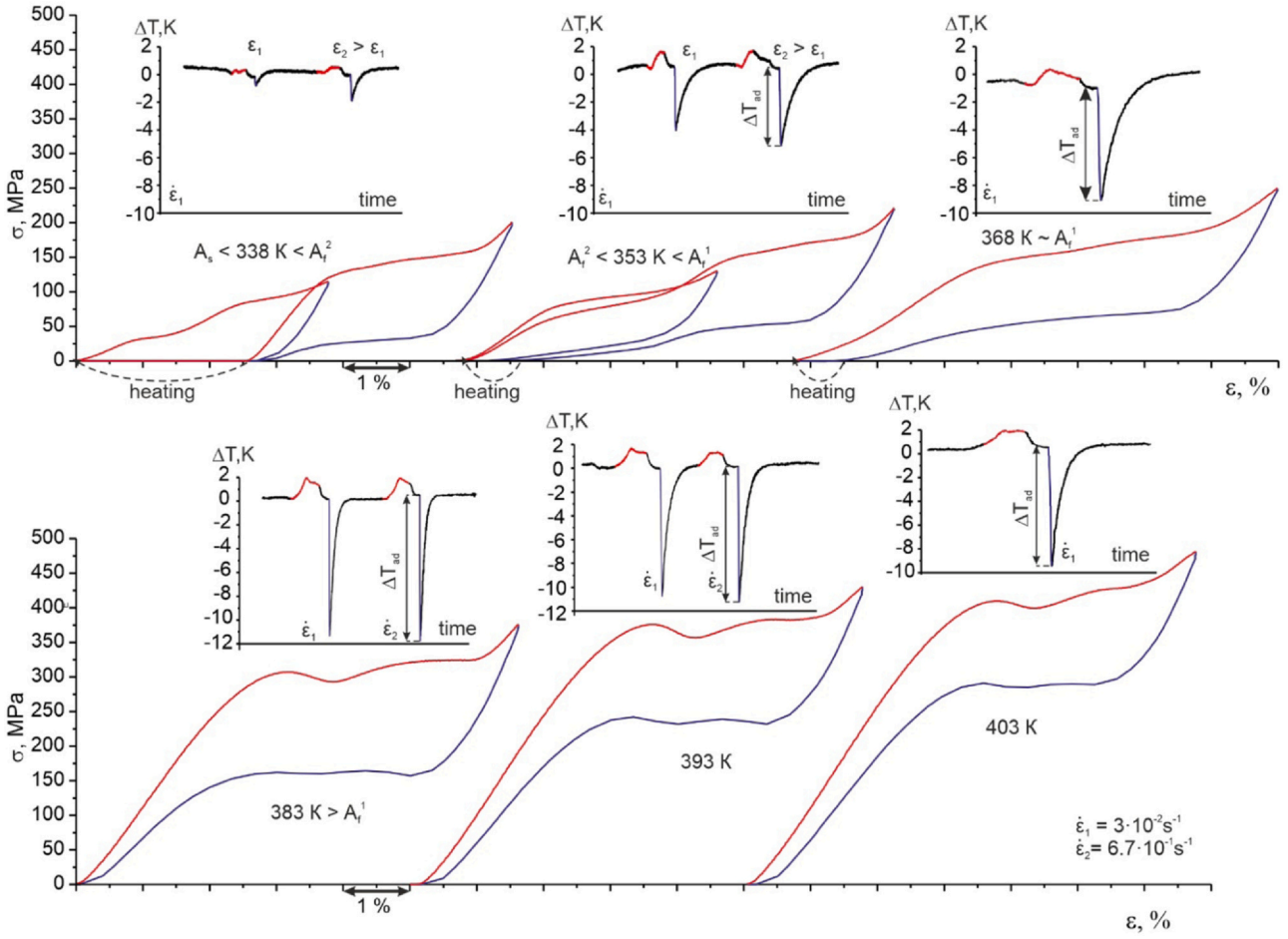

Fig. 4. σ(ε) curves and corresponding sample temperature change as a function of time ΔT(t) in the loading/unloading cycles for [011]-oriented $Ni_{50}Mn_{30}Ga_{20}$ single crystals in compression.

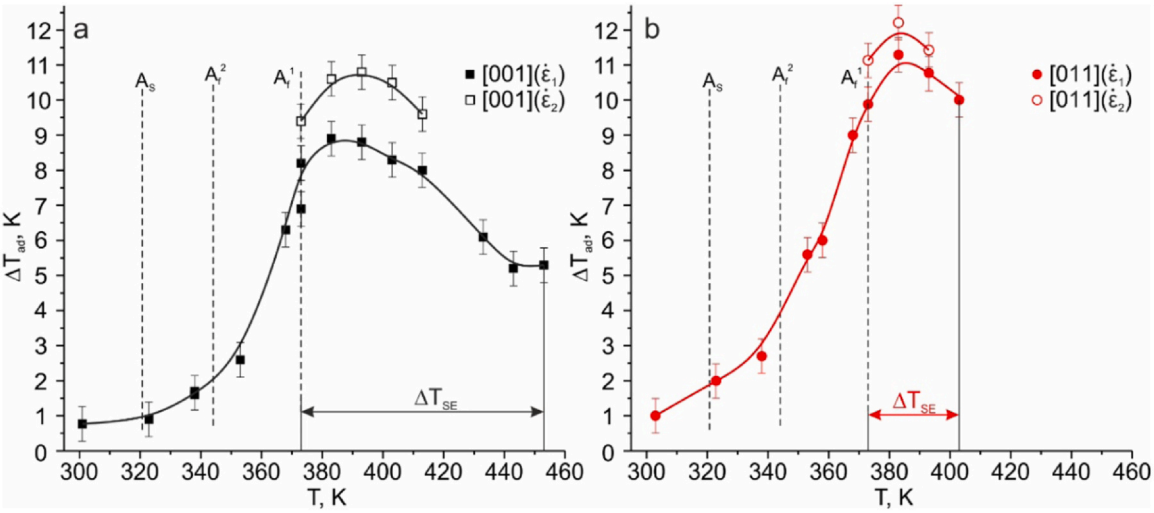

Fig. 5. The temperature dependence of the adiabatic temperature change ΔT_{ad} for [001] - (a) and [011] - (b) oriented $Ni_{50}Mn_{30}Ga_{20}$ single crystals.

Table 2
Theoretical ΔT_{ad} (max) and experimental ΔT_{ad}(exp) values of the adiabatic temperature change, coefficient of performance COP of $Ni_{50}Mn_{30}Ga_{20}$ single crystals.

Orientation	ΔH^{M-A}, J/g	ΔT_{ad} (max), K	ΔT_{ad} (exp), K		COP	
			$\dot{\varepsilon}_1$	$\dot{\varepsilon}_2$	$\dot{\varepsilon}_1$	$\dot{\varepsilon}_2$
[001]	7.1	14.5	8.9	10.8	20.4	25.8
[011]			11.3	12.3	8.0	9.2

comparison with the [011]-oriented crystals, where the change of ΔT_{ad} with the unloading rate was weaker (9%). This experimental result can be explained by different kinetics of reverse MT at loading/unloading cycles depending on crystal orientation. The reverse MT is observed in a wide interval of deforming stresses (e.g., from 308 MPa to 103 MPa at T_t = 403 K) in [001]-oriented crystals, where the detwinning of $L1_0$-martensite under stress is absent. The same kinetics occurs in [001]-oriented crystals during MT in stress-assisted cooling/heating cycles: a higher stress level results in a wider MT temperature interval (Fig. 7a). This defines the strong dependence of adiabatic temperature change ΔT_{ad} on the unloading rate in [001]-oriented single crystals.

In contrast, the detwinning of $L1_0$-martensite under stress, which is observed in [011]-oriented single crystals, leads to deviation of the habit plane from its invariant position, wide stress hysteresis and formation of reverse MT at almost constant stresses (e.g., $\sigma \approx 285$ MPa at T_t = 403 K) (Fig. 4). Such "burst-like" kinetics of reverse MT in [011]-oriented single crystals was confirmed to be observed in stress-induced cooling/heating MT (Fig. 7b) as well as in the other [011]-oriented single crystals of Heusler alloys [19,20,24]. Thus, at loading/unloading cycles in [011]-oriented crystals, the reverse MT at unloading possessed almost "burst-like" kinetics and occurred after achieving a constant stress level. In this case, therefore, the ΔT_{ad} value weakly depended on the unloading rate.

In previous research [2,6], ΔT_{ad} at loading/unloading cycles was inversely proportional to energy dissipation, which can be a characteristic of stress hysteresis. In the present work in $Ni_{50}Mn_{30}Ga_{20}$ single crystals, the strong influence of energy dissipation (stress hysteresis) on ΔT_{ad} at loading/unloading cycles was not observed. First, the maximum ΔT_{ad} values for [001]- and [011]-oriented crystals were close (10.8 and 12.3, respectively) despite more than twofold difference in stress hysteresis values (Table 2). The lower value of adiabatic temperature change ΔT_{ad} = 10.8 K (T_t = 393 K, $\dot{\varepsilon}_2 = 6.7 \cdot 10^{-1}$ s^{-1}) was observed in [001]-oriented crystals with narrow stress hysteresis $\Delta\sigma$ = 51 MPa compared with [011]-oriented crystals, where SE was characterized by wide stress hysteresis $\Delta\sigma$ = 142 MPa and larger ΔT_{ad} = 12.3 K (T_t = 383 K, $\dot{\varepsilon}_2 = 6.7 \cdot 10^{-1}$ s^{-1}).

Second, a 45% reduction of the ΔT_{ad} with the increase in test temperature was observed in [001]-oriented single crystals, while

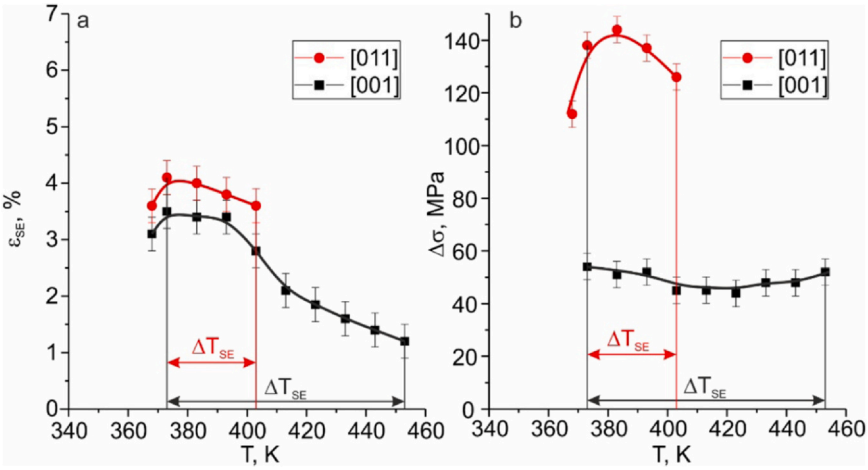

Fig. 6. The temperature dependences of transformation strain ε_{SE} (a) and the stress hysteresis $\Delta\sigma$ (b) for $Ni_{50}Mn_{30}Ga_{20}$ single crystals.

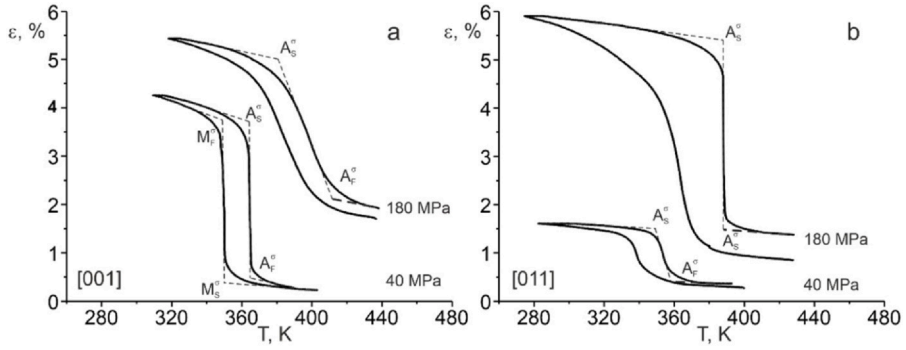

Fig. 7. The ε(T) response at stress-assisted cooling/heating cycles for [001]- (a) and [011]- (b) $Ni_{50}Mn_{30}Ga_{20}$ single crystals.

the stress hysteresis remained the same Δσ = 50 ÷ 60 MPa (Figs. 5a and 6b). Consequently, stress hysteresis was not shown to define the ΔT_{ad}.

However, the energy dissipation (and the stress hysteresis) defines the efficiency of the ECE for application in the work cycle. The COP can be used to classify the elastocaloric properties of materials in terms of application efficiency. This coefficient is equal to the ratio of the useful thermal energy, which can be absorbed by the sample from the environment during cooling, to the value of energy dissipation, which characterizes the work spent ($\oint \sigma d\varepsilon$) for the loading/unloading cycle [25,26]:

$$COP = \frac{C_p \Delta T_{ad}}{1/\rho \oint \sigma d\varepsilon}, \quad (2)$$

where ρ – density (6500 kg·m^{-3}). The value of this coefficient achieved 25.8 and 9.2 for single crystals in this study along [001]- and [011]-directions in compression, respectively (Table 2). As was shown in previous research [1,6,25,26], the maximum COP values (20–25) were observed in CuZnAl and TiNiCu shape memory alloys in tension; however, the COP value did not exceed 20 in compression (14.2 for the CuZnAl alloy, ~13 for the NiFeGaCo alloy, ~7 for $Ni_{44.8}Mn_{36.9}In_{13.3}Co_{5.0}$ and ~17 for TiNi). The [001]-oriented $Ni_{50}Mn_{30}Ga_{20}$ single crystals, therefore, possessed the largest COP coefficient of 25.8 among shape memory alloys in compression and thus have a high potential to be used in solid-state cooling devices.

4. Conclusions

It was experimentally shown in this study that as-grown $Ni_{50}Mn_{30}Ga_{20}$ single crystals possess a weak orientation dependence of adiabatic temperature change ΔT_{ad} in compression. The maximum values of ΔT_{ad} equal 8.9 (10.8) K along [001]-direction and 11.3 (12.3) K along [011]-direction with the unloading rates of $3.3 \cdot 10^{-2}$ s^{-1} and $6.7 \cdot 10^{-1}$ s^{-1}, respectively. The experimental maximum ΔT_{ad} values are close to the theoretical estimation of material cooling ability ΔT_{ad} (max) = 14.5 K, which was obtained from DSC data during MT at stress-free cooling/heating cycles.

The temperature interval of efficient cooling ability in $Ni_{50}Mn_{30}Ga_{20}$ single crystals is defined by the temperature interval of SE and strongly depends on the crystal orientation: the working temperature interval for [001]-oriented crystals is 80 K, which is in 2.67 times larger than the interval for [011]-oriented crystals (30 K).

The dependence of adiabatic temperature change ΔT_{ad} on the strain rate was shown to be defined by the kinetics of reverse MT and the crystal orientation. The "burst-like" kinetics of reverse MT in [011]-oriented $Ni_{50}Mn_{30}Ga_{20}$ single crystals, where the detwinning of $L1_0$-martensite under stress is present, defines the weak dependence of the ΔT_{ad} on the strain rate. In contrast, [001]-oriented crystals are characterized by both the wide temperature interval of MT in cooling/heating cycles under constant stress and a high deformation strengthening coefficient θ, which causes the much stronger dependence of ΔT_{ad} on the strain rate due to the absence of $L1_0$-martensite detwinning during forward stress-induced MT.

Strong orientation dependence of stress hysteresis Δσ in $Ni_{50}Mn_{30}Ga_{20}$ single crystals defines the orientation dependence of COP for applications. The results showed that [011]-oriented single crystals are characterized by wide stress hysteresis Δσ = 110 ÷ 142 MPa and low COP = 9.2. The narrow stress hysteresis Δσ = 50 ÷ 60 MPa in [001]-oriented $Ni_{50}Mn_{30}Ga_{20}$ single crystals produce the maximum COP value (25.8) among shape memory alloys, indicating the high potential for the application of their elastocaloric properties.

CRediT authorship contribution statement

N.Yu. Surikov: Conceptualization, Investigation, Validation, Formal analysis, Writing - original draft, Writing - review & editing. **E.Yu. Panchenko:** Conceptualization, Writing - review & editing, Project administration, Funding acquisition. **E.E. Timofeeva:** Methodology, Writing - review & editing. **A.I. Tagiltsev:** Validation, Writing - review & editing. **Yu.I. Chumlyakov:** Conceptualization, Resources, Supervision.

Declaration of Competing Interest

The authors declare that they have no known competing financial interests or personal relationships that could have appeared to influence the work reported in this paper.

Acknowledgements

The reported study was supported by Russian Science Foundation, Russia (project No. 20-19-00153). The electron microscopy studies were carried out on the equipment of the Krasnoyarsk Regional Center for Collective Use of the FRC KSC SB RAS.

References

[1] S. Qian, Y. Geng, Y. Wang, J. Ling, Y. Hwang, R. Radermacher, I. Takeuchi, J. Cui, A review of elastocaloric cooling: materials, cycles and system integrations, Int. J. Refrig. 64 (2016) 1–19, https://doi.org/10.1016/j.ijrefrig.2015.12.001
[2] H. Sehitoglu, Y. Wu, E. Ertekin, Elastocaloric effects in the extreme, Scr. Mater. 148 (2018) 122–126, https://doi.org/10.1016/j.scriptamat.2017.05.017
[3] G.J. Pataky, E. Ertekin, H. Sehitoglu, Elastocaloric cooling potential of NiTi, Ni_2FeGa, and CoNiAl, Acta Mater. 96 (2015) 420–427, https://doi.org/10.1016/j.actamat.2015.06.011
[4] J. Guo, Z. Wei, Y. Shen, Y. Zhang, J. Li, X. Hou, J. Liu, Low-temperature superelasticity and elastocaloric effect in textured Ni–Mn–Ga–Cu shape memory alloys, Scr. Mater. 185 (2020) 56–60, https://doi.org/10.1016/j.scriptamat.2020.04.007
[5] L. Wei, X. Zhang, W. Gan, C. Ding, L. Geng, Hot extrusion approach to enhance the cyclic stability of elastocaloric effect in polycrystalline Ni-Mn-Ga alloys, Scr. Mater. 168 (2019) 28–32, https://doi.org/10.1016/j.scriptamat.2019.04.009

[6] Y. Wu, E. Ertekin, H. Sehitoglu, Elastocaloric cooling capacity of shape memory alloys – role of deformation temperatures, mechanical cycling, stress hysteresis and inhomogeneity of transformation, Acta Mater. 135 (2017) 158–176, https://doi.org/10.1016/j.actamat.2017.06.012
[7] J. Wang, Q. Yu, K. Xu, C. Zhang, Y. Wu, C. Jiang, Large room-temperature elastocaloric effect of $Ni_{57}Mn_{18}Ga_{21}In_4$ alloy undergoing a magnetostructural coupling transition, Scr. Mater. 130 (2017) 148–151, https://doi.org/10.1016/j.scriptamat.2016.11.024
[8] D. Li, Z. Li, J. Yang, Z. Li, B. Yang, H. Yan, D. Wang, L. Hou, X. Li, Y. Zhang, C. Esling, X. Zhao, L. Zuo, Large elastocaloric effect driven by stress-induced two-step structural transformation in a directionally solidified $Ni_{55}Mn_{18}Ga_{27}$ alloy, Scr. Mater. 163 (2019) 116–120, https://doi.org/10.1016/j.scriptamat.2019.01.014
[9] D. Zhao, F. Xiao, Z. Nie, D. Cong, W. Sun, J. Liu, Burst-like superelasticity and elastocaloric effect in [011] oriented $Ni_{50}Fe_{19}Ga_{27}Co_4$ single crystals, Scr. Mater. 149 (2018) 6–10, https://doi.org/10.1016/j.scriptamat.2018.01.029
[10] E.E. Timofeeva, E.Y. Panchenko, N.G. Vetoshkina, Y.I. Chumlyakov, A.I. Tagiltsev, A.S. Eftifeeva, H. Maier, The mechanism of orientation dependence of cyclic stability of superelesticity in NiFeGaCo single crystals under compression, Russ. Phys. J. 59 (2016) 1251–1260, https://doi.org/10.1007/s11182-016-0899-0
[11] Y.H. Qu, D.Y. Cong, S.H. Li, W.Y. Gui, Z.H. Nie, M.H. Zhang, Y. Ren, Y.D. Wang, Simultaneously achieved large reversible elastocaloric and magnetocaloric effects and their coupling in a magnetic shape memory alloy, Acta Mater. 151 (2018) 41–55, https://doi.org/10.1016/j.actamat.2018.03.031
[12] G.W.H. Hohne, W. Hemminger, H.-J. Flammersheim, Differential Scanning Calorimetry: An Introduction for Practitioners, Springer-Verlag, New York, 1996, https://doi.org/10.1007/978-3-662-03302-9
[13] T.E. Bucheit, S.L. Kumpf, J.A. Wert, Modeling the stress-induced transformation behavior of shape memory alloy single crystals, Acta Mater. 43 (1995) 4189–4199, https://doi.org/10.1016/0956-7151(95)00105-5
[14] J. Dadda, H.J. Maier, D. Niklasch, I. Karaman, H.E. Karaca, Y.I. Chumlyakov, Pseudoelasticity and cyclic stability in $Co_{49}Ni_{21}Ga_{30}$ shape-memory alloy single crystals at ambient temperature, Metall. Mater. Trans. 39A (2008) 2026–2039, https://doi.org/10.1007/s11661-008-9543-0
[15] C. Jiang, G. Feng, S. Gong, H. Xu, Effect of Ni excess on phase transformation temperatures of NiMnGa alloys, Mater. Sci. Eng. A 342 (2003) 231–235, https://doi.org/10.1016/S0921-5093(02)00288-5
[16] V.A. Chernenko, J. Pons, E. Cesari, K. Ishikawa, Stress–temperature phase diagram of a ferromagnetic Ni–Mn–Ga shape memory alloy, Acta Mater. 53 (2005) 5071–5077, https://doi.org/10.1016/j.actamat.2005.07.018
[17] X. Sun, J. Song, X. Zhang, C. Xie, Thermal cycling behaviors of the intermartensitic transformation in a polycrystalline $Ni_{52.5}Mn_{23.7}Ga_{23.8}$ alloy, J. Alloy. Compd. 509 (2011) 4868–4870, https://doi.org/10.1016/j.jallcom.2011.01.191
[18] P. Entel, M.E. Gruner, M. Acet, A. Çakır, R. Arróyave, T. Duong, S. Sahoo, S. Fähler, V.V. Sokolovskiy, Properties and decomposition of Heusler alloys, Energy Technol. 6 (2018) 1478–1490, https://doi.org/10.1002/ente.201800256
[19] C. Jiang, Y. Muhammad, L. Deng, W. Wu, H. Xu, Composition dependence on the martensitic structures of the Mn-rich NiMnGa alloys, Acta Mater. 52 (2004) 2779–2785, https://doi.org/10.1016/j.actamat.2004.02.024
[20] L. Wei, X. Zhang, J. Liu, L. Geng, Orientation dependent cyclic stability of the elastocaloric effect in textured Ni-Mn-Ga alloys, AIP Adv. 8 (2018) 055312, https://doi.org/10.1063/1.5028212
[21] X. Xu, T. Kanomata, R. Kainuma, Specific heat and entropy change during martensitic transformationin $Ni_{50}Mn_{50-x}Ga_x$ ferromagnetic shape memory alloys, Acta Mater. 79 (2014) 159–167, https://doi.org/10.1016/j.actamat.2014.06.036
[22] Y. Hu, Z. Li, B. Yang, S. Qian, W. Gan, Y. Gong, Y. Li, D. Zhao, J. Liu, X. Zhao, L. Zuo, D. Wang, Y. Du, Combined caloric effects in a multiferroic Ni–Mn–Ga alloy with broad refrigeration temperature region, APL Mater. 5 (2017) 046103, https://doi.org/10.1063/1.4980161
[23] E. Panchenko, Y. Chumlyakov, H.J. Maier, E. Timofeeva, I. Karaman, Tension/compression asymmetry of functional properties in [001]-oriented ferromagnetic NiFeGaCo single crystals, Intermetallics 18 (2010) 2458–2463, https://doi.org/10.1016/j.intermet.2010.09.009
[24] E. Panchenko, et al., Thermoelastic martensitic transformations in [011]-oriented Ni49Fe18Ga27Co6 single crystals under tension and compression loads, AIP Conf. Proc. 1909 (2017) e020165.
[25] J. Tušek, K. Engelbrecht, L. Mañosa, E. Vives, N. Pryds, Understanding the thermodynamic properties of the elastocaloric effect through experimentation and modelling, Shap. Mem. Superelasticity 2 (2016) 317–329, https://doi.org/10.1007/s40830-016-0094-8
[26] B. Lu, M. Song, Z. Zhou, W. Liu, B. Wang, S. Lu, C. Wu, L. Yang, J. Liu, Reducing mechanical hysteresis via tuning the microstructural orientations in Heusler-type $Ni_{44.8}Mn_{36.9}In13_{.3}Co_{5.0}$ elastocaloric alloys, J. Alloy. Compd. 785 (2019) 1023–1029, https://doi.org/10.1016/j.jallcom.2019.01.276